

# Temporal evolution and alternation of mechanisms of electric-field-induced patterns at ultralow-frequency driving

Nándor Éber,<sup>1</sup> Laura O. Palomares,<sup>1</sup> Péter Salamon,<sup>1</sup> Alexei Krehkov,<sup>2</sup> and Ágnes Buka<sup>1</sup>

<sup>1</sup>Institute for Solid State Physics and Optics, Wigner Research Centre for Physics, Hungarian Academy of Sciences, H-1525 Budapest, P.O.B. 49, Hungary

<sup>2</sup>Institute of Physics, University of Bayreuth, D-95440 Bayreuth, Germany

(Received 11 April 2012; published 14 August 2012)

The temporal evolution of patterns within the driving period of the ac voltage was studied in the 10-mHz–250-Hz frequency range. It was shown that the stationary electroconvection pattern of the conductive regime transforms into a flashing one at ultralow frequencies, existing only in narrow time windows within the period. Furthermore a transition between electroconvection and flexoelectric domains was detected which is repeating in each half period. The two patterns are well separated in time and in Fourier space. Simultaneous current measurements uncovered that the electric properties of the polyimide orienting layers influence the redistribution of the applied voltage. The experimental findings are in good qualitative agreement with the theoretical predictions based on an extended standard model including flexoelectricity.

DOI: 10.1103/PhysRevE.86.021702

PACS number(s): 61.30.Gd, 47.54.–r

## I. INTRODUCTION

Applying an electric field onto a planarly oriented thin layer of an anisotropic fluid (in particular a nematic liquid crystal) often leads to the appearance of spatially periodic structures—stripe patterns [1–4]. These patterns exhibit a richness in their morphology (the magnitude and the direction of the wave vector) as well as in the mechanism of formation, depending on the material, control, and system parameters.

Electroconvection (EC) rolls [3] and flexoelectric domains [4–8] (or shortly flexodomains) are long known examples of such patterns. While electroconvection is a paradigm for a nonequilibrium, dissipative pattern forming process occurring in suitable nematics at a wide frequency range of driving voltages (from dc to several kHz), flexodomains (FDs) correspond to an equilibrium deformation observed for specific material parameter combinations mostly at dc or at very low frequency (below a few Hz) ac voltages. Both pattern types have extensively been studied experimentally in the past decades, mostly with optical microscopy which is sensitive to the spatial variation of the director. It has been found that various pattern types are immediately distinguishable by the direction of their wave vector  $\mathbf{q}$ ; flexodomains are stripes running parallel with the initial director  $\mathbf{n}_0$  (defined by the surface alignment), while EC rolls are typically either perpendicular to  $\mathbf{n}_0$  (normal rolls) or make some angle with it (oblique rolls).

The theoretical interpretation of FDs is relatively easy; being an equilibrium deformation, its characteristics could be obtained via the minimization of the free energy of the system. It has first been shown by Bobylev and Pikin [4,6] using a one-elastic-constant approximation and dc driving that flexoelectricity is responsible for the appearance of flexodomains; they obtained analytical formulas for the threshold voltage  $V_{FD}$  and the critical wave number  $q_{FD}$  of the pattern. This description has recently been extended taking into account the anisotropy of elasticity and ac driving [9].

Explanation of the occurrence of EC patterns requires more massive theoretical tools, as besides director distortions they

also involve flow and separation of space charges [10,11]. The combination of the equations of nematohydrodynamics and electrodynamics, with the simplifying assumption of Ohmic electrical conductivity, yielded the so-called standard model (SM) of electroconvection [12]. The SM could interpret the appearance and the onset characteristics [the frequency dependence of the threshold voltage  $V_c(f)$  and the critical wave vector  $\mathbf{q}_c(f)$ ] of the most typical EC morphologies (which have been coined standard EC patterns). Recently the SM has been extended by including flexoelectricity into the description [13]. This, on the one hand, gave corrections to  $V_c(f)$  and  $\mathbf{q}_c(f)$  and thus resulted in a better quantitative agreement with the experiments on standard EC patterns; on the other hand, it uncovered the pattern forming mechanism for some nonstandard EC patterns where the SM could not give an explanation.

Switching on or off the voltage applied to the sample the patterns does not appear or disappear instantaneously; there are characteristic times for their growth or decay which are related to the sample thickness  $d$  and to some material parameters. The (extended) SM includes phenomena evolving on different time scales:  $\tau_d$ ,  $\tau_q$ , and  $\tau_v$ , corresponding to the relaxation of the director, the charges, and the flow, respectively ( $\tau_q$  and  $\tau_v$  are irrelevant for flexodomains). Typically  $\tau_d \gg \tau_q \gg \tau_v$ , and growth or decay times are in the order of  $\tau_d$  [14,15]. When driven by ac voltages, there is another characteristic time, the period  $T = 1/f$  of the driving sine wave of frequency  $f$ .

Most experiments on EC and theoretical analyses of the SM have been carried out in the frequency range where  $\tau_d \gg T$  (for  $d = 10 \mu\text{m}$  and typical material parameters it corresponds to  $f > 10 \text{ Hz}$ ). Calculations have shown that in the case of ac driving the SM equations may have solutions with two different time symmetries: the relevant quantities (like the director component  $n_z$  normal to the cell surface, etc.) either change or do not change their sign when time is shifted by half a period ( $t \rightarrow t + T/2$ ) [3,9,13]. The solutions with  $\langle n_z(t) \rangle \neq 0$  and  $\langle n_z(t) \rangle = 0$  are called the conductive and the dielectric modes, respectively (here  $\langle \rangle$  denotes averaging over the full period  $T$ ). The two modes possess different  $V_c(f)$  and  $\mathbf{q}_c(f)$  values.

In the experiments typically that mode is observable which has the lower  $V_c$ . Therefore, at the frequency  $f_c$  where the two  $V_c(f)$  curves intersect, a crossover should occur. Indeed, such transitions between the conductive EC mode at  $f < f_c$  and the dielectric mode at  $f > f_c$  were often observed in the experiments.

The time symmetry mentioned above implies that in the dielectric mode  $n_z$  changes its sign twice in each period, i.e., there are time instants repeatedly where the system returns to the initial undistorted state. In contrast to that, in the conductive regime the sign of  $n_z$  does not change with time; only small, higher harmonic, oscillations of the director are allowed around a stationary value. This temporal behavior of the two distinct EC modes has been tested and justified experimentally by independent techniques: light diffraction [16] and optical microscopy with stroboscopic illumination [17,18] or using fast digital (line) cameras [19–21].

Experiments at low driving frequencies are very scarce. Some morphological transitions with voltage and temperature have been reported in the 1–30-Hz range, but without attention to the temporal behavior [22]. Recently May *et al.* [23] have studied the dielectric EC mode in a nematic with very low conductivity at extreme low frequencies ( $f < 1$  Hz) where  $\tau_d \ll T$ . They have observed as expected that the EC pattern flashes: i.e., evolves and decays within each half period of the driving voltage. Moreover, it has been found that there is another flashing pattern, corresponding to the flexodomains (FDs), which also appears in each half period; thus there is a repetitive transition between the pattern types.

The main goal of the present paper is to prove that nematics with a conductive EC mode, where  $\langle n_z \rangle \neq 0$ , surprisingly exhibit similar scenarios at low  $f$ . These experimental findings are in full agreement with recent theoretical calculations [9] using the extended SM, which have justified that the flashing behavior at  $\tau_d \ll T$  is general. Any pattern can exist only in part of the half period; moreover, the time windows for the appearance of patterns of different types are shifted with respect to each other.

The paper is organized in the following way. After introducing our experimental setup and methods in Sec. II, we present the experimental results in Sec. III. First we focus on the frequency dependence of the pattern morphology and temporal behavior, followed by addressing the peculiarities of the extreme low  $f$  driving in detail. Then we report the results of simultaneous current measurement which uncovered that the electric properties of the alignment layers influence the redistribution of the applied voltage. The results are analyzed and compared to the theoretical expectations in Sec. IV and the paper is finally closed with a summary of the results and conclusions in Sec. V.

## II. EXPERIMENTAL SETUP AND EVALUATION METHOD

Experiments have been carried out on planarly aligned samples of the nematic mixture Phase 5 (Merck). This compound has a negative dielectric and positive conductivity anisotropy, and has often served as a reference compound for studying standard EC.

The nematic was filled into a commercial cell (E.H.C. Co.) of thickness  $d = 11.3\ \mu\text{m}$ . Its temperature was held at

$T = 30 \pm 0.05^\circ\text{C}$  using an Instec HSi hot stage driven by an mK-1 temperature controller PC board. The sinusoidal ac voltage applied to the cell was provided by an Agilent 33120A function generator through a high voltage amplifier. The applied voltage and the current flowing through the cell was monitored by a digital oscilloscope (TiePie Handyscope HS3).

The voltage-induced patterns were observed by a LEICA DM RX polarizing microscope at white light illumination using the single polarizer (shadowgraph) technique. An attached high speed camera EoSens MC1362 allowed recording snapshot sequences at a variable (maximum 2000 frames/s) rate with a spatial resolution of  $512 \times 512$  pixels at 256 grey levels. A specially designed trigger logic was applied to synchronize image recording with the negative zero crossing of the applied voltage. Thus the temporal behavior could be monitored by taking 20–4000 snapshots (depending on the frequency) within a driving period.

The recorded images were evaluated by digital image processing in order to obtain the time evolution of the pattern contrast  $C(t)$ . As a simplest definition of the contrast we have taken the mean square deviation of the intensity,  $C = \langle (I_{ij} - \langle I_{ij} \rangle)^2 \rangle$  (here  $I_{ij}$  is the intensity of a pixel, and  $\langle \rangle$  denotes averaging over the whole image). Though this definition does not allow distinguishing between various pattern morphologies (in contrast to the power spectrum of a two-dimensional fast Fourier transformation (FFT), selective to a pattern mode with a given  $\mathbf{q}$  as used in Ref. [23]), it satisfactorily discriminates the initial (undistorted) and the patterned state.

The contrast defined above has  $C_0 \neq 0$  value even for the initial undistorted state (at no applied voltage), which will be regarded as a background value. It originates from inhomogeneities of the initial planar state (e.g., from thermal fluctuations always present in a planar nematic). When comparing image sequences recorded at different frequencies, we will also use a background subtracted normalized contrast, defined as  $(C - C_0)/(C_{\max} - C_0)$  where  $C_{\max}$  denotes the maximal contrast within the driving period.

## III. EXPERIMENTAL RESULTS

### A. Pattern characteristics

The patterns induced by an applied voltage have been investigated in a wide (10 mHz–250 Hz) frequency range where EC occurs as primary instability. At the low frequency end though the transition to flexodomains can be detected. Phase 5 is a widely investigated material for EC studies and it is known that the threshold morphologies follow the SM predictions; thus one observes normal rolls in the dielectric regime and just below the crossover frequency  $f_c$  in the conductive regime. Below the Lifshitz point ( $f_L$ ) oblique rolls occur with a continuously increasing tilt angle as the frequency decreases.

Figure 1 plots the measured EC threshold voltage  $V_c$  (rms values) versus the driving frequency on a logarithmic scale. The crossover between the dielectric and conductive EC modes occurred at  $f_c \approx 230$  Hz. In the conductive regime  $V_c(f)$  shows the typical (expected) behavior [3] with a bending down at very low  $f$  as reported recently [24]. It is also seen that  $V_c(f)$  has a minimum at about 200 mHz; the voltage to be

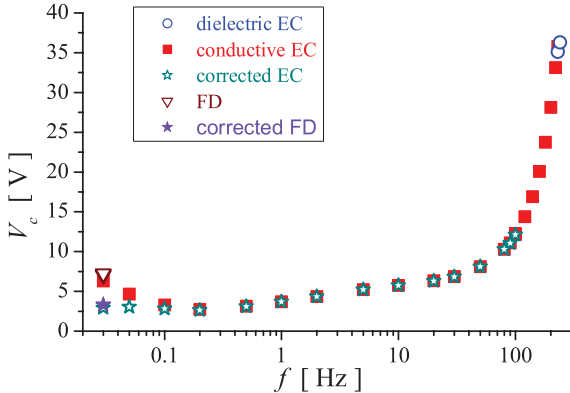


FIG. 1. (Color online) The measured frequency dependence of the EC threshold voltage  $V_c$  on a logarithmic scale. Open stars correspond to a corrected threshold value (see text in Sec. IV). The threshold for flexodomains and its corrected value is also indicated at low  $f$ .

applied to the cell for inducing the pattern increases as  $f$  is reduced further. This behavior will be discussed in more detail in Sec. IV.

The threshold  $V_{FD}$  for FD is also shown in Fig. 1 for the specific frequency of 30 mHz, where it has been studied in detail. Though not yet measured precisely, there are indications that the frequency dependence of  $V_{FD}$  is weaker than that of  $V_c$ ; thus one expects a crossover of the  $V_{FD}(f)$  and  $V_c(f)$  curves below 30 mHz. This is reinforced by the fact that FD could, but standard EC rolls could not be detected in the sample at pure dc applied voltages.

As already mentioned in Sec. I, EC has recently been experimentally studied for very low frequencies [23] in a system which exhibits dielectric regime in the entire range. The time symmetry of the solution in the dielectric regime implies that the director component  $n_z$  oscillates with the driving voltage [ $V \propto \sin(2\pi t/T)$ ]; thus the transmitted light intensity (contrast) is expected to follow a  $\propto \sin^2(2\pi t/T)$  behavior, leading to the extinction of the pattern twice within the period. This has been verified in Ref. [23] for high frequencies. Decreasing the frequency and approaching the range where  $\tau_d$  becomes comparable with  $T$ , one expects and observes deviations from the  $\sin^2(2\pi t/T)$  dependence which finally results in a scenario where the pattern exists only in a very narrow time window, twice within the period (spiky contrast).

The situation is different in our system presented here, because it exhibits the conductive mode in almost the entire frequency range studied (especially at low  $f$ ). Its time symmetry implies (for  $T \ll \tau_d$ ) a steady director deformation profile in leading order with a small sinusoidal  $2f$  modulation, resulting in a basically steady contrast in time. In order to explore whether or how this behavior changes at lowering  $f$ , we have followed the temporal evolution of the contrast as a function of the frequency. This is shown in Fig. 2 which depicts the normalized contrast for a time interval of one period in the case of four selected frequencies (100, 10, 1, and 0.1 Hz) covering three decades; the starting instant  $t = 0$  corresponds to the negative zero crossing of the applied sine wave.

It is immediately perceptible that, in agreement with the expectations, at high frequency ( $f = 100$  Hz) the contrast is

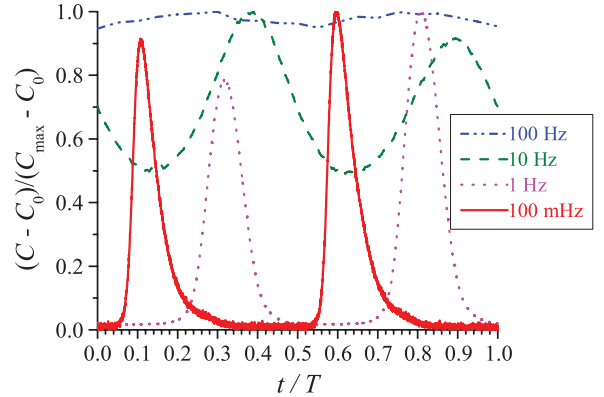


FIG. 2. (Color online) The measured temporal evolution of the normalized contrast within one period at different driving frequencies.

nearly constant. Reducing  $f$  first the amplitude of the  $2f$  modulation becomes larger, then the contrast minimum  $C_{\min}$  reaches the background value ( $C_0$ ) and surprisingly the spiky character appears here too. The intuitive explanation is that when  $T$  approaches the director relaxation time, the director has time to relax within the period (at least partially). Then, though the time symmetry of the conductive mode persists even for low  $f$ , it cannot yield a stationary director any more.

We demonstrate the transition from the steady contrast to the spiky behavior also in Fig. 3, where the frequency dependence of the relative contrast modulation is plotted. As seen from the figure, the transition between the stationary ( $\Delta C \approx 0$ ) and the spiky ( $\Delta C \approx 1$ ) regime occurs in the  $1 \text{ Hz} < f < 30 \text{ Hz}$  range. Using the known material parameter set of Phase 5 [24,25], one obtains  $\tau_d = 0.147 \text{ s}$  for the studied cell. The corresponding frequency,  $\tau_d^{-1} = 6.8 \text{ Hz}$ , falls in the middle of the transition frequency range, indicating that the change of the behavior is related to the director relaxation time.

Now we concentrate on the very low frequency behavior where the EC contrast is spiky. The voltage dependence of the scenarios is demonstrated at an ultralow driving frequency of  $f = 30 \text{ mHz}$  in Fig. 4, exhibiting the temporal evolution of the contrast  $C(t)$  within a driving period where  $0 \leq t \leq T/2$  corresponds to the negative and  $T/2 \leq t \leq T$  to the positive half period of the applied voltage.

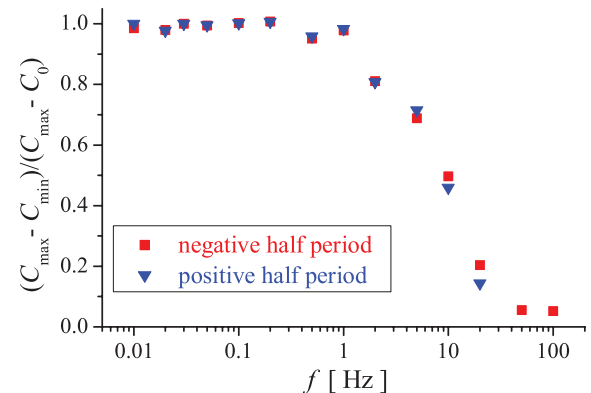


FIG. 3. (Color online) Frequency dependence of the relative contrast modulation.

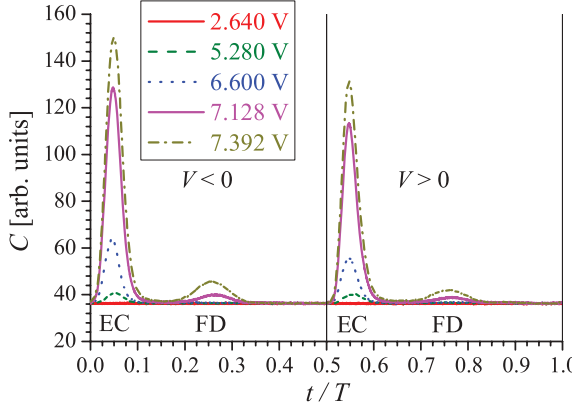


FIG. 4. (Color online) The measured temporal variation of the pattern contrast within the driving period  $T$  at various driving voltages  $V$ .  $T = 30^\circ\text{C}$ ,  $f = 30\text{ mHz}$ .

At low voltages there is no pattern; the contrast is constant. Applying a voltage exceeding the EC threshold spikes appear with their maximum located at  $t_{\text{EC}} = 0.05T$  and  $t_{\text{EC}} = 0.55T$  indicating the onset of the instability; their maximum contrast increases with the voltage. At even higher voltages a second set of spikes emerge with their maximum at  $t_{\text{FD}} = 0.26T$  and  $t_{\text{FD}} = 0.76T$ , indicating the appearance of the FD pattern. In between the spikes the contrast falls back to the background value, i.e., the patterns emerge and decay periodically, with a period of  $T/2$ .

We note that the  $C(t)$  curve did not depend on whether it was recorded immediately after applying the voltage (in the first period) or later (after 50 periods).

Figure 5 shows the snapshots of the patterns detected. We have identified the first spike at  $t_{\text{EC}} = 0.05T$  as conductive electroconvecting oblique rolls [Fig. 5(a)], while the second spike at  $t_{\text{FD}} = 0.26T$  belongs to the parallel stripes of the flexodomains [Fig. 5(b)].

We note that, according to Fig. 4, the two half periods do not seem to be equivalent in a sense that the amplitudes of the contrast spikes for  $V > 0$  are smaller than for  $V < 0$ . This polarity dependence indicates some asymmetry of the bounding plates or of the driving, to be discussed later in Sec. IV.

Besides the amplitudes of the spikes, their location ( $t_{\text{EC}}$  and  $t_{\text{FD}}$ ) within the half period is also of interest. It is evident

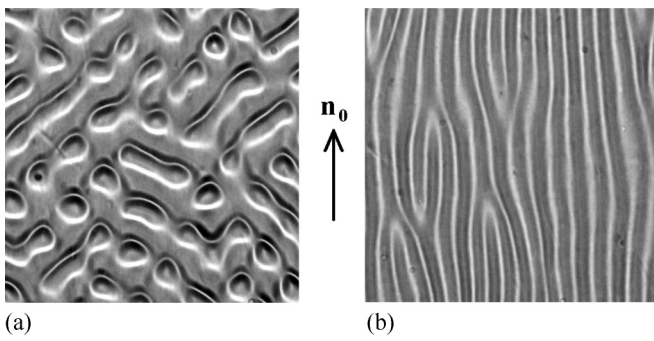


FIG. 5. Snapshots of the patterns observed within the same half period. (a) EC oblique rolls; (b) flexodomains. The initial director  $\mathbf{n}_0$  is denoted by an arrow.

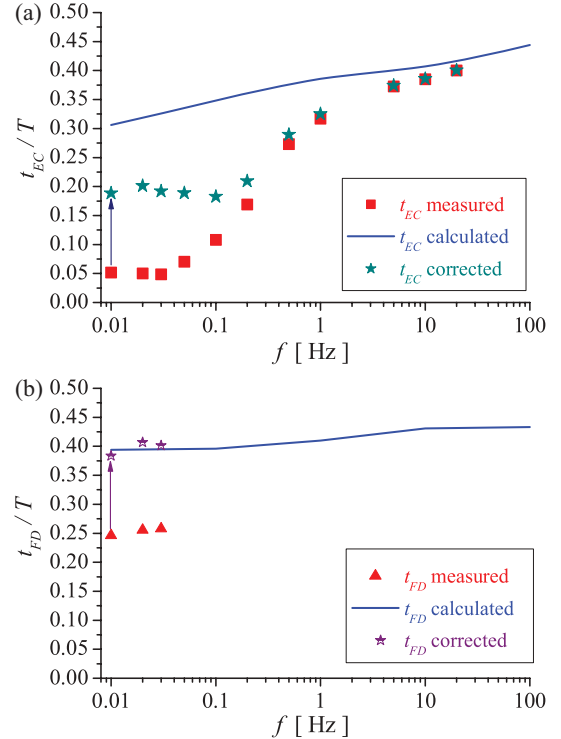


FIG. 6. (Color online) Frequency dependence of the measured (solid symbols) and calculated (solid curves) location of contrast maxima for the (a) EC patterns, (b) flexodomains. Star symbols indicate corrected values (see explanation text in Sec. IV).

from Fig. 4 that the locations of the EC contrast maxima,  $t_{\text{EC}}$ , do not coincide with the maxima of the applied voltage, as one would naively expect for an ultralow-frequency driving. It has been found that the EC spikes are symmetric and the location of their centers is almost independent of the voltage;  $t_{\text{EC}} = (0.048 \pm 0.002)T + nT/2$  in the voltage range of  $V_c < V < 8.2\text{ V}$ . In contrast to that, the location of the flexospike,  $t_{\text{FD}}$ , was found to decrease with growing voltage; from  $t_{\text{FD}} = (0.263 \pm 0.003)T + nT/2$  at onset it reduces to  $t_{\text{FD}} = (0.22 \pm 0.01)T + nT/2$  at  $V = 8.2\text{ V}$ .

It can be seen already in Fig. 2 that the spike positions depend on the driving frequency too. This is shown in more detail in Fig. 6(a) which exhibits  $t_{\text{EC}}/T$  versus  $f$  measured at voltages slightly above the threshold. One can notice that the shift is substantial;  $t_{\text{EC}}$  reduces from  $0.40T$  at high  $f$  to about  $0.05T$  in the ultralow  $f$  spiky regime.

As the spike positions are strongly frequency dependent, the question arises whether the width of the time window of the spiky pattern changes with  $f$ . The half width of the spike, i.e., the time interval  $\Delta t$  during which the contrast  $C$  is larger than  $(C_{\max} + C_0)/2$ , can be used as a comparative measure. Figure 7 plots  $\Delta t/T$  for the frequency range of the spiky regime ( $f < 1\text{ Hz}$ ). It is found that  $\Delta t/T$  reduces slightly, i.e., the EC spikes become narrower, when  $f$  is lowered. (We note that for  $f > 1\text{ Hz}$  one finds  $C_{\min} > C_0$ , i.e., the pattern does not decay fully; the pattern becomes contrast modulated but not spiky.)

Let us now focus on the frequency dependence of the flexodomains. One has to note first that flexodomains exist in a much narrower frequency range than the EC pattern.

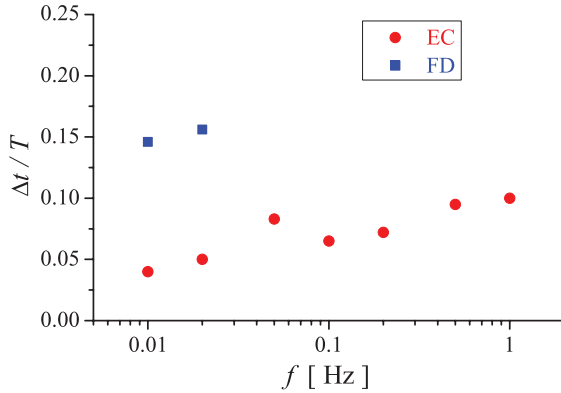


FIG. 7. (Color online) Frequency dependence of the half width of the EC and flexodomain spikes.

Second, the clear separation of the EC and FD spikes in time is observable only at around 30 mHz and below. The positions of the flexodomain spikes ( $t_{\text{FD}}$ ) are plotted in Fig. 6(b). This figure will further be discussed in Sec. IV. The half width of the flexodomain spikes seem to be larger than those of the EC ones (Fig. 7).

At slightly higher (but still low) frequencies, where  $T$  becomes shorter and  $V_{\text{FD}} - V_c$  is larger, the EC pattern does not decay fully before the flexodomains appear; rather a gradual rotation of the rolls occurs from the oblique EC ones toward the parallel stripes of the flexodomains. This is illustrated in Fig. 8 by the  $C(t)$  curves recorded for voltages below  $V_c$ , slightly above  $V_c$  and above  $V_{\text{FD}}$  at  $f = 100$  mHz driving. The flexodomains correspond to the shoulder on the falling edge of  $C(t)$ . Increasing the frequency further, flexodomains could not be identified at all.

### B. Current measurements

In the previous Sec. III A we have demonstrated that the behavior at extreme low frequencies (flashing patterns, alternation between EC and flexodomains) differs strongly from the usual high frequency one. The understanding of these scenarios definitely requires a special attention to other frequency dependent phenomena which might occur simultaneously. Electrical properties belong to those, as a liquid crystal cell can be regarded as a mostly capacitive

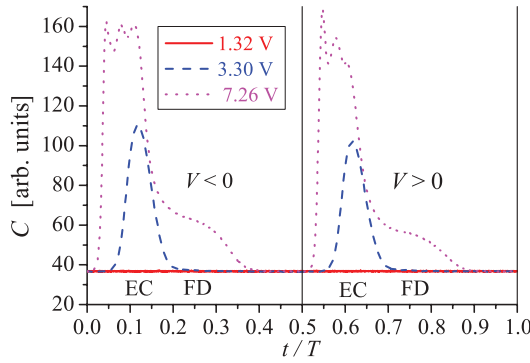


FIG. 8. (Color online) The measured temporal variation of the pattern contrast within the driving period  $T$  at various driving voltages  $V$  at  $f = 100$  mHz.

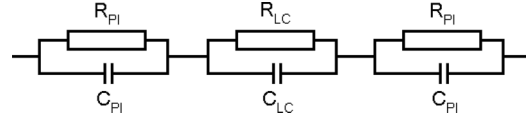


FIG. 9. Low frequency equivalent circuit of the measuring cell. Indices PI and LC refer to the polyimide orienting layer and the liquid crystal, respectively.

impedance at high  $f$ , while mostly resistive as the frequency is reduced to very low values. In addition, while a simple parallel RC circuit is a good equivalent circuit for a liquid crystal cell in the usual ( $10 \text{ Hz} < f < 10 \text{ kHz}$ ) frequency range, this does not hold for the low ( $f < 1 \text{ Hz}$ ) frequency range due to the presence of the orienting layer. The planar orientation is provided by rubbed polyimide (PI) films which are fairly good insulators. They themselves should be represented by a parallel RC circuit which is connected in series with the parallel RC of the liquid crystal (LC). The resulting improved equivalent circuit, shown in Fig. 9, has been in use for a long time in low frequency dielectric spectroscopy [26,27].

In order to prove the relevance of the modified equivalent circuit for our experimental conditions and to allow estimation of the impedance values of the PI and LC layers, the current flowing through the cell in response to the sinusoidal applied voltage has been monitored simultaneously to image-recording in the 10-mHz–100-Hz frequency range.

At high frequency the wave form of the current signal is sinusoidal, just as that of the applied voltage. As the capacitive part of the current dominates over the Ohmic part, the current  $I$  has a phase delay of  $\phi \approx \pi/2$  with respect to the applied voltage. Lowering the frequency one observes a decrease of the current, as expected; this is accompanied by a change in the phase delay as plotted in Fig. 10 by square symbols. It shows that  $\phi$  does not change monotonically with the frequency. This behavior is quite well reproducible with the equivalent circuit in Fig. 9, as shown by the solid curve in Fig. 10 which was obtained assuming realistic values for the resistances and capacitances:  $R_{\text{PI}} = 70 \text{ M}\Omega$ ,  $C_{\text{PI}} = 379 \text{ nF}$ ,  $R_{\text{LC}} = 16 \text{ M}\Omega$ ,  $C_{\text{LC}} = 400 \text{ pF}$ .

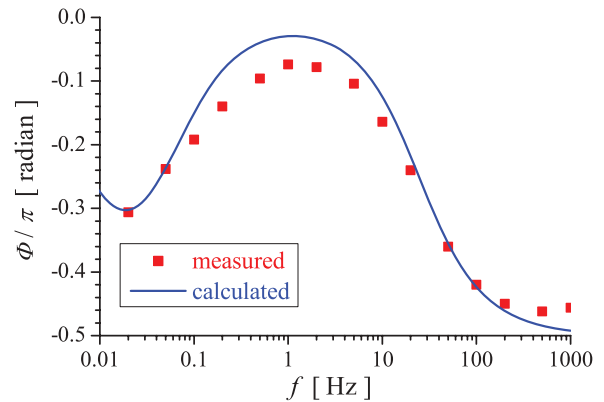


FIG. 10. (Color online) Frequency dependence of the phase of the current with respect to the applied voltage. Squares represent measured values, the solid line is a calculation based on the electrical equivalent circuit in Fig. 9.

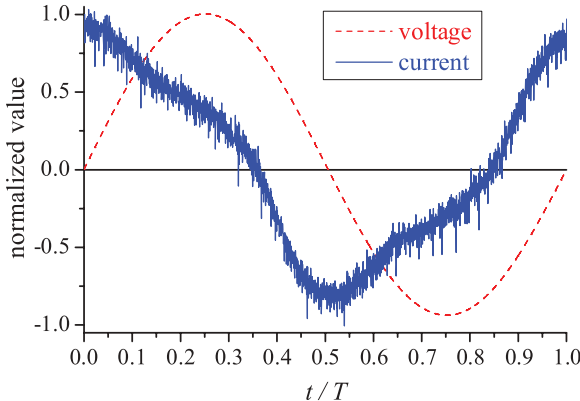


FIG. 11. (Color online) The wave forms of the applied voltage (sinusoidal) and the current response (distorted) at  $f = 20$  mHz.

As a consequence of the equivalent circuit in Fig. 9, the voltage on the liquid crystal differs from the applied voltage both in magnitude and phase. This has to be taken into account by proper corrections in Figs. 1 and 6 which are going to be discussed in detail later in Sec. IV.

One has to mention, however, that even the modified equivalent circuit of Fig. 9 is just a simplification of the real situation, as it does not take into account the effects related to the ionic conductivity of liquid crystals (e.g., ionic screening, nonlinear  $I(V)$  characteristics, etc.) which become especially important at low frequencies. As an indication of those additional effects Fig. 11 exhibits the distorted wave form of the current obtained as a response to the sinusoidal applied voltage at  $f = 20$  mHz. We note here that the deviation from the sinusoidal shape depicted in Fig. 11 is not due to the appearance of the patterns; the response was recorded at  $V = 1.25$  V, i.e., much below the threshold voltage.

In order to provide a more complete description of these phenomena, the measured current signal should be fitted by the nonlinear model for the ionic current [28], which, due to the complexity of the model, is a challenging task.

#### IV. COMPARISON WITH THEORY

The experimental findings presented in Sec. III A and in Ref. [23] have unambiguously proved that at ultralow  $f$  driving the electric-field-induced patterns have a spiky character, independent of whether they are of equilibrium type (like flexodomains) or of dissipative ones (conductive or dielectric EC mode).

The extended SM including flexoelectricity, which has been developed recently [9], is able to describe both types of patterns. We have also performed numerical calculations for EC and FD using this model. The results presented here have been obtained from a linear stability analysis of the nematoelectrohydrodynamic equations for the planar basic state under the action of an applied ac voltage, as described in detail in Ref. [13]. At the substrates strong planar anchoring for the director and no-slip boundary conditions for the velocity were assumed. The material parameters of Phase 5 were taken from [24], except the electrical conductivity and the flexoelectric coefficients. The conductivity was adjusted to reproduce the experimental crossover frequency  $f_c$ , while the

flexocoefficients were chosen to match the FD wavelength observed at dc voltages. The set of parameters used provide a satisfactory fitting of the former  $V_c(f)$  curves as well as of the FD wavelength; this indicates that, as it has been pointed out in [24], the determination of the flexocoefficients solely from the threshold curves of EC is not unique.

In Fig. 12(a) the temporal evolution of the director perturbation  $n_z$  at the midplane of the sample is shown for a single period of various driving frequencies. Though the relation between the pattern amplitude (i.e.,  $n_z$  in the midplane) and the optical contrast (as defined in Sec. II) is by far not trivial and may be different for different pattern types [23], it is clear that a larger  $n_z$  would yield a higher contrast (at least near the onset where  $n_z$  is small). Thus  $n_z(t)$  in Fig. 12(a) is in a nice accordance with the experimental contrast curves shown in Fig. 2, reproducing all experimental features from the nearly steady state at high  $f$  to the spiky behavior at the lowest  $f$ .

The equations for FD form a subset of the EC equations, which can be obtained by making the conductivity as well as the flow velocities zero. The temporal evolution of  $n_z$  in FD calculated by the linear stability analysis is presented in Fig. 12(b). The behavior is similar to that of the EC case: there are spikes at very low  $f$ , however, at high  $f$  it approaches a state with a  $2f$  modulation of fairly large amplitude. Note that for  $f > 10$  Hz FD has higher threshold than EC; thus the temporal evolution of the director shown in Fig. 12(b) cannot be observed experimentally.

Let us now compare the time windows of existence for the two types of patterns in their spiky regime. Figures 13(a) and 13(b) plot the calculated normalized  $n_z(t)$  for EC as well as for FD at the ultralow  $f = 10$  mHz and at the still low  $f = 100$  mHz, respectively. It is evident from the figures that the theory predicts different time windows for the two patterns. The predicted sequence of events coincides with the observations: after each zero crossing of the voltage EC comes first and FD evolves later, i.e.,  $t_{\text{EC}} < t_{\text{FD}}$ . Moreover, Fig. 13(a) clearly shows that at an ultralow frequency EC decays before FD appears, in full agreement with the experiments (see Fig. 4). For higher frequency, however, the calculated time windows for EC and FD partially overlap as shown in Fig. 13(b). This might be the reason that at the same (100 mHz) frequency a clear separation of EC and FD could not be observed experimentally (see Fig. 8).

Note that the calculated  $n_z(t)$  curves shown in Figs. 12 and 13 were normalized to the maxima of  $n_z$ . The reason is that while the linear stability analysis allows us to obtain the onset characteristics of various pattern modes, it leaves the pattern amplitude (the maximum of  $n_z$ ) undetermined. A description of the voltage dependence of  $n_z$  or the transformation of one pattern into the other at a fixed voltage much above the threshold would require a nonlinear analysis of the problem. In addition, at a quantitative comparison with experiments (e.g., with Figs. 4 or 8) one should take into account that the shadowgraph response, i.e., the relation between the optical contrast and  $n_z$ , may be different for the two types of patterns [23].

From the calculated  $n_z(t)$  curves  $t_{\text{EC}}$  and  $t_{\text{FD}}$  can easily be obtained as the positions of the maxima. These are shown as calculated values in Figs. 6(a) and 6(b) by solid curves. The data indicate that both  $t_{\text{EC}}$  and  $t_{\text{FD}}$  decrease at reducing  $f$ ,

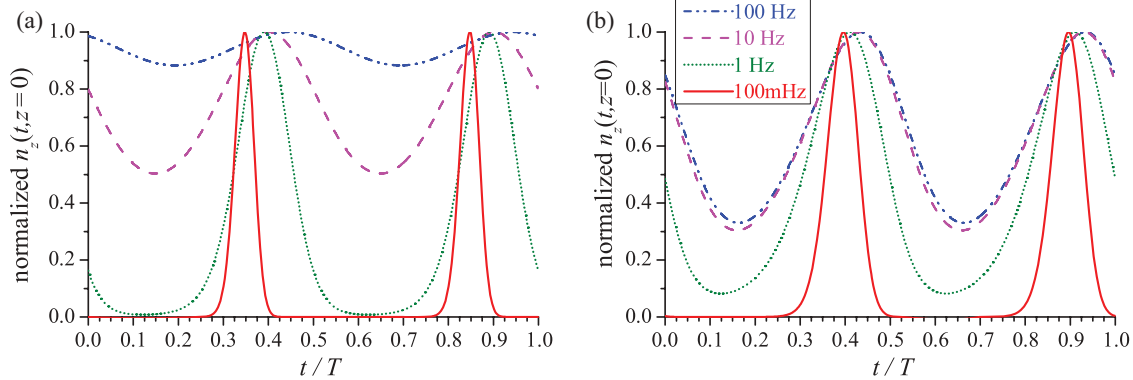


FIG. 12. (Color online) Temporal evolution of the calculated director component  $n_z$  in the midplane of the sample within one period at different driving frequencies (a) for a conductive EC pattern and (b) for flexodomains.

however, the slope of  $t_{EC}$  is larger and increases compared to that of  $t_{FD}$  as  $f$  is lowered.

While the theory reproduces the experimental findings qualitatively, there seems to be a quantitative mismatch in the location of the spikes. While at  $f = 10$  Hz the theoretical and experimental  $t_{EC}$  still coincide, it is seen in Fig. 6 that there is a growing difference between the two values below 1 Hz. Also the measured  $t_{FD}$  seems to be much lower than expected from the theory.

We claim, however, that this mismatch is mostly apparent. It is due to the fact that experimentally  $t_{EC}$  and  $t_{FD}$  are measured with respect to the zero crossing of the voltage applied to the cell, while the theoretical values are given with respect to the zero crossing of the voltage on the liquid crystal in the cell (this latter is not accessible experimentally). The current measurements have proven that the experimental cell is better represented by the equivalent circuit shown in Fig. 9 than with a simple RC circuit. It implies that there is an internal voltage attenuation which becomes important at low frequencies: the voltage on the liquid crystal is less than the applied voltage and is phase shifted by  $\phi$  with respect to it. Using the same impedance values which reproduced approximately the phase of the current, the internal attenuation and phase shift could be obtained. Taking these into account the threshold voltage (on the LC film only) and the spike positions (with respect to the zero crossing of the voltage on the LC) could be recalculated. These corrected values are also plotted in Figs. 1, 6(a), and

6(b) by star symbols. One can notice in Fig. 1 that the internal voltage attenuation is quite substantial at the lowest  $f$ . The same applies for the phase shift as well, as seen in Fig. 6. It is also perceptible that the phase corrected experimental  $t_{FD}$  values already correspond to the theoretical  $t_{FD}(t)$  dependence and the mismatch of  $t_{EC}$  is also reduced substantially.

We should note, however, that the theoretical description by the extended SM does not involve ionic processes which are unambiguously present at low frequencies, as shown by the current response in Fig. 11. Similarly shaped current response to low frequency sinusoidal driving due to ionic contribution can be found in the theoretical work of Derfel [28]. Inclusion of ionic effects into our model might result in better agreement for  $t_{EC}$ .

We should still address the polarity dependence observed in Fig. 4. The theoretical description by the extended SM assumes a symmetric cell with ideal planar boundary conditions; then no polarity dependence is predicted, as can actually be seen in Figs. 12 and 13. The planar orientation in real cells is provided by antiparallelly rubbed polyimide layers; they typically have some small pretilt ( $2\text{--}5^\circ$ ). The full identity of the two bounding electrode plates (in pretilt, anchoring strength, ionic adsorption, etc.) is, moreover, not guaranteed. In addition, as the cells had to be driven by dc amplifiers due to the ultralow frequencies used, the presence of a small dc offset voltage  $V_o$  on the cell cannot be excluded. These factors in combination with the linear (therefore polarity dependent)

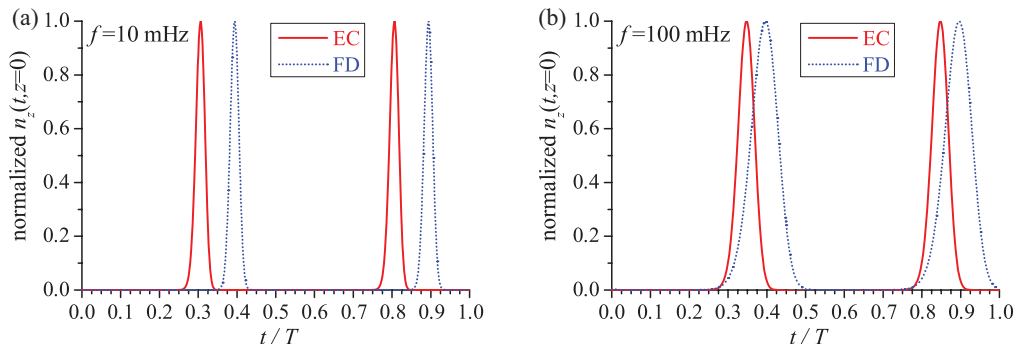


FIG. 13. (Color online) Temporal evolution of the calculated director component  $n_z$  for EC and FD in the midplane of the sample within one period (a) at  $f = 10$  mHz and (b) at  $f = 100$  mHz.

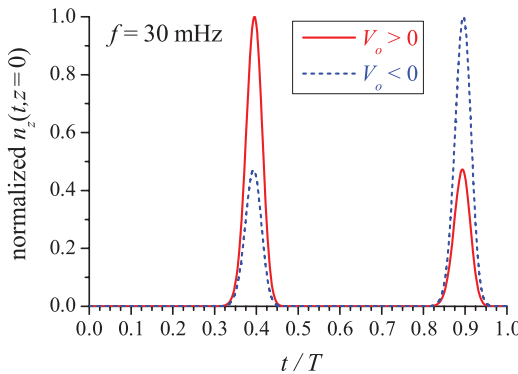


FIG. 14. (Color online) Temporal evolution of the calculated director component  $n_z$  for flexodomains in the midplane of the sample within one period of the driving ac voltage at dc offset voltages of opposite polarity.

flexoelectric interaction may lead to the break of symmetry. Though a precise theoretical analysis of all these factors could not be performed, the effect of a dc offset voltage on FD could be analyzed. Figure 14 shows the  $n_z(t)$  curves calculated with a small dc offset voltage of  $V_o = \pm 50$  mV. The heights of the  $n_z$  spikes differ substantially in the two half periods. It can also be seen that the small and the big spikes interchange if the polarity of the offset voltage is reversed. Note the extreme sensitivity: the  $V_o$  used in the calculation is less than 1% of  $V_{FD}$ .

Finally we mention that the magnitude of the electrical conductivity seems to be an important factor in the scenarios described. In samples with larger conductivity the time window for the occurrence of the EC pattern was

substantially wider, occasionally including also that of the flexodomains.

## V. SUMMARY

The character of the standard electroconvection patterns in the conductive regime changes substantially when the frequency becomes much lower than the inverse director relaxation time. Instead of remaining stationary as at high  $f$ , the pattern evolves and decays within each half period of the driving at ultralow  $f$ . Flexoelectric domains have a similar flashing character in the same frequency range. This behavior is in accordance with the theoretical predictions of the extended standard model of electroconvection.

It has also been found that at this low-frequency range the internal attenuation caused by the insulating polyimide orienting layer becomes non-negligible resulting in a reduction and phase shifting of the actual voltage sensed by the liquid crystal layer compared to the voltage applied to the cell. Considering this correction brings the experimental values of the time windows of pattern existence closer to theoretical predictions.

As at ultralow  $f$  the two types of patterns are well separated, not only in the Fourier space but also in time, a repetitive morphological transition occurs between them in each half period. A theoretical description of this transition, especially considering the possible interactions between the two patterns, requires further theoretical developments.

## ACKNOWLEDGMENTS

Financial support by the Hungarian Research Fund OTKA K81250 is gratefully acknowledged. L.O.P. is grateful for the support provided by CONACYT (Mexico).

- 
- [1] L. M. Blinov and V. G. Chigrinov, *Electrooptic Effects in Liquid Crystal Materials* (Springer, New York, 1996).
  - [2] P. G. de Gennes and J. Prost, *The Physics of Liquid Crystals* (Oxford Science Publications, New York, 2001).
  - [3] L. Kramer and W. Pesch, in *Pattern Formation in Liquid Crystals*, edited by Á. Buka, and L. Kramer (Springer-Verlag, New York, 1996), pp. 221–256.
  - [4] S. A. Pikin, *Structural Transformations in Liquid Crystals* (Gordon and Breach Science Publishers, New York, 1991).
  - [5] L. K. Vistin, Sov. Phys. Crystallogr. **15**, 514 (1970) [Kristallofrafija **15**, 594 (1970)].
  - [6] Yu. P. Bobylev and S. A. Pikin, Sov. Phys. JETP **45**, 195 (1977) [Zh. Eksp. Teor. Fiz. **72**, 369 (1977)].
  - [7] M. I. Barnik, L. M. Blinov, A. N. Trufanov, and B. A. Umanski, Sov. Phys. JETP **46**, 1016 (1977) [Zh. Eksp. Teor. Fiz. **73**, 1936 (1977)].
  - [8] M. I. Barnik, L. M. Blinov, A. N. Trufanov, and B. A. Umanski, J. Phys. (France) **39**, 417 (1978).
  - [9] A. Krekhov, W. Pesch, and Á. Buka, Phys. Rev. E **83**, 051706 (2011).
  - [10] E. F. Carr, Mol. Cryst. Liq. Cryst. **7**, 253 (1969).
  - [11] W. Helfrich, J. Chem. Phys. **51**, 4092 (1969).
  - [12] E. Bodenschatz, W. Zimmermann, and L. Kramer, J. Phys. (France) **49**, 1875 (1988).
  - [13] A. Krekhov, W. Pesch, N. Éber, T. Tóth-Katona, and Á. Buka, Phys. Rev. E **77**, 021705 (2008).
  - [14] N. Éber, S. A. Rozanski, S. Németh, Á. Buka, W. Pesch, and L. Kramer, Phys. Rev. E **70**, 061706 (2004).
  - [15] W. Pesch, L. Kramer, N. Éber, and Á. Buka, Phys. Rev. E **73**, 061705 (2006).
  - [16] T. Tóth-Katona, N. Éber, and Á. Buka, Phys. Rev. E **83**, 061704 (2011).
  - [17] U. Schneider, M. de la Torre Juárez, W. Zimmermann, and I. Rehberg, Phys. Rev. A **46**, 1009 (1992).
  - [18] S. Messlinger, A. Sack, W. Schöpf, and I. Rehberg, Presentation at the 35th Topical Meeting on Liquid Crystals, Bayreuth, 21–23 March 2007, Book of Abstracts p. P37.
  - [19] H. Amm, M. Grigutsch, and R. Stannarius, Z. Naturforsch. A **53**, 117 (1998).
  - [20] H. Amm, M. Grigutsch, and R. Stannarius, Mol. Cryst. Liq. Cryst. **320**, 11 (1998).

- [21] T. John, J. Heuer, and R. Stannarius, *Phys. Rev. E* **71**, 056307 (2005).
- [22] Y. Xiang, Y.-K. Liu, X.-S. Xie, J.-M. Li, J.-H. Wang, and Z.-G. Cai, *Appl. Phys. Lett.* **97**, 203507 (2010).
- [23] M. May, W. Schöpf, I. Rehberg, A. Krekhov, and A. Buka, *Phys. Rev. E* **78**, 046215 (2008).
- [24] T. Tóth-Katona, N. Éber, Á. Buka, and A. Krekhov, *Phys. Rev. E* **78**, 036306 (2008).
- [25] M. Treiber, N. Éber, Á. Buka, and L. Kramer, *J. Phys. II France* **7**, 649 (1997).
- [26] A. Golovin, Introduction to Dielectric Measurements of Nematic Liquid Crystals, [http://www.lci.kent.edu/Lavrentovich/Introduction\\_to\\_dielectric\\_measurments2.htm](http://www.lci.kent.edu/Lavrentovich/Introduction_to_dielectric_measurments2.htm).
- [27] A. Abderrahmen, F. Fekih Romdhane, H. Ben Ouada and A. Gharbi, *Sci. Technol. Adv. Mater.* **9**, 025001 (2008).
- [28] G. Derfel, *J. Mol. Liq.* **144**, 59 (2009).